PB93-228773

THREE-DIMENSIONAL DEFORMATION PROCESS SIMULATION WITH EXPLICIT USE OF POLYCRYSTALLINE PLASTICITY MODELS

THINKING MACHINES CORP.
CAMBRIDGE, MA

FEB 92

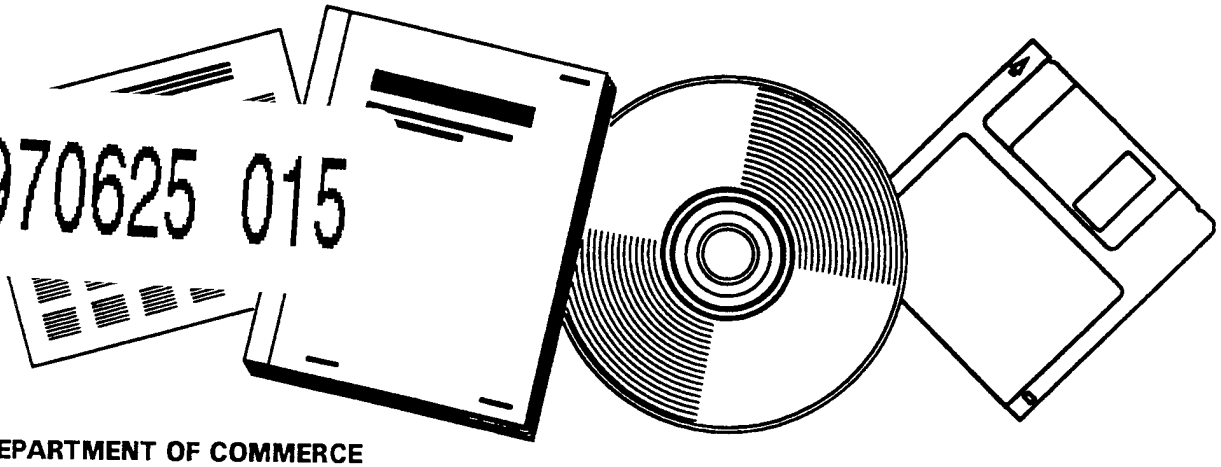

U.S. DEPARTMENT OF COMMERCE
National Technical Information Service

Three-Dimensional Deformation Process Simulation with Explicit Use of Polycrystalline Plasticity Models

A. Beaudoin, P. Dawson, Cornell University
K. Mathur, Thinking Machines Corporation
G. Johnson, University of California, Berkeley

Thinking Machines Corporation

Technical Report Series

251

REPORT DOCUMENTATION PAGE

PB93-228773

1. AGENCY USE ONLY (Leave blank)	2. REPORT DATE	3. REPORT TYPE AND DATES COVERED
	20, Feb. 1992	Technical

4. TITLE AND SUBTITLE
Three-dimensional deformation process simulation with explicit use of polycrystalline plasticity models

5. FUNDING NUMBERS
Office of Navel Research
N00014-90-J-1810

6. AUTHOR(S)
A. Beaudoin, P. Dawson, K. Mathur, and G. Johnson

7. PERFORMING ORGANIZATION NAME(S) AND ADDRESS(ES)
Thinking Machines Corp.
245 First Street
Cambridge, MA 02142-1264

8. PERFORMING ORGANIZATION REPORT NUMBER
TMC-251

9. SPONSORING/MONITORING AGENCY NAME(S) AND ADDRESS(ES)

10. SPONSORING/MONITORING AGENCY REPORT NUMBER

11. SUPPLEMENTARY NOTES

12a. DISTRIBUTION/AVAILABILITY STATEMENT

12b. DISTRIBUTION CODE

13. ABSTRACT (Maximum 200 words)

The comination of massive parallel processing and polycrystalline plasticity theory offers the potential for applying detailed microstructural models to macroscopic deformation processes. In this work the finite element method is used to solve for the three-dimensional deformation of a plastic workpiece. The interaction of the material symmetry pole ~~figure~~ adopted in analysis of pole figures and the boundry conditions posed in the plasticity boundry value problem is examined. It is shown that the use of spatially distinct aggregates in a material experiencing local kinematic inhomogeneities throughout its deformation history leads to texture predictions which compare favorably with experimental measurements.

14. SUBJECT TERMS	15. NUMBER OF PAGES	16. PRICE CODE
	50	

17. SECURITY CLASSIFICATION OF REPORT	18. SECURITY CLASSIFICATION OF THIS PAGE	19. SECURITY CLASSIFICATION OF ABSTRACT	20. LIMITATION OF ABSTRACT
Unclassified	SAR	SAR	SAR

Three-Dimensional Deformation Process Simulation with Explicit Use of Polycrystalline Plasticity Models

A. J. Beaudoin *
K. K. Mathur †
P. R. Dawson ‡
G. C. Johnson §

February 20, 1992

Abstract

The combination of massive parallel processing and polycrystalline plasticity theory offers the potential for applying detailed microstructural models to macroscopic deformation processes. In this work the finite element method is used to solve for the three-dimensional deformation of a plastic workpiece. The elemental constitutive response is derived from the microstructural response of a polycrystal aggregate situated in the element. Crystal orientations and their respective weighted contributions to the aggregate response are selected to approximate the orientation distribution derived from experimental pole figure measurements. The interaction of the material symmetry adopted in analysis of pole figures and the boundary conditions posed in the plasticity boundary value problem is examined. Through the

*Graduate Research Assistant, Sibley School of Mechanical and Aerospace Engineering, Cornell University, Ithaca, NY 14853

†Scientist, Thinking Machines Corporation, Cambridge, Mass.

‡Professor, Sibley School of Mechanical and Aerospace Engineering, Cornell University, Ithaca, NY 14853

§Professor, University of California, Berkeley

introduction of distinct aggregates with decreasing crystal to aggregate ratio, an inhomogeneous material response is developed where: 1) the orientation distribution becomes well approximated only by a collection of spatially distinct aggregates, and 2) these aggregates experience deformation paths of increasing variation. It is shown that the use of spatially distinct aggregates in a material experiencing local kinematic inhomogeneities throughout its deformation history leads to texture predictions which compare favorably with experimental measurements.

Running header: Process Simulation using Polycrystalline Models

Nomenclature

a - constant in slip system constitutive relation
$\boldsymbol{C}$ - fourth order tensor mapping deformation rate to stress
$\boldsymbol{C}^c$ - fourth order mapping tensor in a crystal
$\overline{\boldsymbol{C}}$ - fourth order mapping tensor in crystal reference frame
$[C]$ - 5×5 matrix representation of $\boldsymbol{C}$
$\boldsymbol{D}$ - symmetric part of velocity gradient
$\boldsymbol{D}'$ - deviatoric portion of $\boldsymbol{D}$
$\boldsymbol{D}^c$ - symmetric part of velocity gradient in a crystal
$\overline{\boldsymbol{D}}$ - symmetric part of velocity gradient in crystal reference frame
$\{f\}$ - discretized external force vector
$\boldsymbol{F}$ - deformation gradient
$\boldsymbol{F}^c$ - deformation gradient in a crystal
$\boldsymbol{F}^p$ - plastic portion of the kinematic decomposition of the crystal deformation gradient
$\mathcal{F}$ - Orientation Distribution Function
H - hardening function for the mechanical threshold
g - orientation in Euler space, $g = (\psi, \theta, \phi)$
g_c - crystal orientation
Δg_c - volume associated with orientation g_c
$[G]$ - incompressibility constraint submatrix of FEM discretization
$[K_D]$ - deviatoric stiffness submatrix of FEM discretization
$\boldsymbol{L}$ - velocity gradient
$\boldsymbol{L}^c$ - velocity gradient in a crystal
m - exponent in slip system constitutive relation
$[M]$ - mass matrix resulting from consistent penalty method
o - orthorhombic symmetry component operator
O - random variable for the orthorhombic symmetry operation
$\boldsymbol{O}$ - rotation representing an orthorhombic symmetry operation
p - pressure
P - nodal point pressures of FEM discretization
$\boldsymbol{P}^\alpha$ symmetric part of Schmid tensor
$\boldsymbol{Q}^\alpha$ skew part of Schmid tensor
$\boldsymbol{R}^*$ - lattice rotation in the kinematic decomposition of the crystal deformation gradient
$\boldsymbol{T}^\alpha$ - Schmid tensor ($\boldsymbol{\nu}^\alpha \otimes \boldsymbol{\eta}^\alpha$) of the α slip system
$\boldsymbol{u}$ - velocity
$\{U\}$ - nodal point velocity of FEM discretization

v - weighting functions in weak statement

v - weighting functions in weak statement

w_c - crystal weighting factor (weight)

$\boldsymbol{W}$ - skew part of velocity gradient

$\boldsymbol{W}^c$ - skew part of velocity gradient in a crystal

$\boldsymbol{W}^p$ - plastic spin from the kinematic decomposition of the velocity gradient in a crystal

β - Parameter in penalty formulation

$\boldsymbol{\eta}^\alpha$ - normal vector of the α slip system

$\boldsymbol{\nu}^\alpha$ - slip direction vector of the α slip system

$\dot{\gamma}^\alpha$ - shear rate on the α slip system

λ - penalty parameter for incompressibility constraint

$\boldsymbol{\sigma}$ - Cauchy stress

$\boldsymbol{\sigma}'^c$ - deviatoric portion of Cauchy stress in a crystal

$\overline{\boldsymbol{\sigma}'}$ - deviatoric portion of Cauchy stress in crystal reference frame

τ^α - resolved shear stress on the α slip system

$\hat{\tau}$ - slip system threshold

(ψ, θ, ϕ) - Euler angles

(Ψ, Θ, Φ) - random variable uniformly distributed on interval $\left[0, \frac{\pi}{2}\right]$

$a(\cdot,\cdot)$, $b(\cdot,\cdot)$, and $(\cdot,\cdot)$ - symmetric bilinear form on volume

$(\cdot,\cdot)_\Gamma$ - symmetric bilinear form on surface with applied tractions Γ

I Introduction

The continued evolution of computer performance has enabled analysts to simulate increasingly complex problems of inelastic deformation. Improvements in computational resources enable refined treatment of the complexity of a problem associated with the workpiece geometry, the non-linear kinematics developed through the course of deformation, and the material constitutive response. The finite element method offers one possible means of numerically discretizing the equilibrium statements posed in the plasticity problem. Such formulations lead to a series of computations which must be carried out for each element in identical fashion. Traditional finite element implementations conduct elemental calculations in a serial manner: first one, then another, until computations for all elements have been completed. Alternatively, these calculations may be performed in a tandem, or parallel [1], fashion so as to exploit the capabilities of massively parallel computer architectures.

Depending on the constitutive theory adopted, parallelism may extend further to the evaluation of the material behavior at a each finite element computation point. For example, the material response at a computation point may be evaluated by interrogating an aggregate of representative microstructural components. The aggregate response then will stem from collecting individual responses of microstructural components spanning the aggregate. At the microstructural level then, there exists the need to solve repeatedly the constitutive equations dictating the response of each component. There exists significant potential for increasing computational throughput by conducting the microstructural level calculations in parallel.

The direct use of microstructural aggregates for computing macroscopic material properties is one approach to formulating constitutive theories. For many common engineering alloys, several aspects of the plastic response can be determined from knowledge of the orientation distribution of the crystals and their individual response characteristics. Such an approach is especially effective in situations where the deformations are sufficiently severe as to alter the underlying microstructure and thereby modify the macroscopic proper-

[1] In this work, use of the word parallel generally refers to the algorithmic character of computations which enables implementation on a parallel computer architecture.

ties.

In typical metal forming processes the deformations are intentionally large. Accurate simulation of both the process history and the final product properties depend on correctly tracking material response as dictated by the evolution of microstructure. For a simulation to be effective, it therefore becomes necessary to adopt a theoretical framework which provides a link between the microstructural evolution and macroscopic product response. However, for a particular theory to be useful in engineering analyses, a minimal requirement is that the model parameters and state variables be specified so as to accurately describe the initial material properties of the workpiece. Micromechanically based theories offer the potential for describing the evolution of complex behaviors, but increase the burden of state and parameter identification. Parallel computing enables the large-scale application of these very detailed constitutive models. It is important to limit choices to those that satisfy certain engineering requirements:

1. that for an arbitrary sample, all of the state variables can be initialized, and

2. that with existing technologies, the model parameters can be experimentally determined.

Attention is focused here on the large strain plastic deformations of polycrystalline metals in the regime of stress and temperature where crystallographic slip dominates among the possible deformation mechanisms. Polycrystalline plasticity theory has been studied extensively over the past decade, especially for metals with face-centered cubic (FCC) and body-centered cubic (BCC) lattices. Experimental techniques for measuring pole figures representing the distribution of crystallites in a specimen are well developed (WENK [1985]). Analytical methodologies to construct discrete approximations of the orientation distribution from pole figure data are available (BUNGE & ESLING [1985]; MATTHIES & WENK [1985]). As such, constitutive models based on polycrystalline plasticity theory meets our engineering requirements concerning the measurement of parameters and initialization of state. Further, the theory provides the means to compute deformation induced anisotropy based on the evolution of crystallographic texture.

This paper details the methodology for performing analyses of transient forming operations, such as forging or deep drawing, utilizing a finite element

formulation with constitutive behavior derived from polycrystalline plasticity theory. The implementation resulting from the formulation is designed to make effective use of a massively parallel computer architecture.

In the following sections, we emphasize several considerations in applying a microstructurally based constitutive theory to predict the evolution of mechanical properties and its impact on deformation. Specifically,

- the measurement of state and the rendering of its discretized approximation are presented for a rolled aluminum specimen;
- iterative procedures are developed for solution of the finite element system of equations for three-dimensional plastic deformation and the microstructural constitutive behavior;
- for the finite element simulations of compression of the specimen, the necessity for consistency between the specification of macroscopic-level kinematic boundary conditions and symmetry in properties derived from microstructural-level aggregates is reviewed; and,
- comparisons of simulation predictions of texture and deformed geometry are made with experiment.

The effect of spatial inhomogeneity in material properties on specimen deformation is examined. To this end, the availability of massively parallel computing enables the parametric study of overall macroscopic deformational response when local material properties exhibit slight variations from material point to material point. Investigations by HARREN & ASARO [1989] and BECKER [1991] have treated the problems of deformation inhomogeneities at a microstructural scale by discretization of a small number of crystals, 27 and 31, respectively. Deformation of the the microstructure is treated explicity, with compatibility and equilibrium issues addressed through application of the finite element method.

A different approach to the effects of spatial inhomogeneity is taken in the present work. We adopt the framework of an existing microstructural theory, the Taylor model (TAYLOR [1938]). In the present simulations there exists a sufficient number of crystals to characterize the state of the material on a macroscopic scale. Spatial inhomogeneity in the deformation field is achieved through specification of different crystal populations for each of

the microstructural aggregates in the problem domain. A parametric study detailing the implications of spatial inhomogeneity on computed texture is presented.

II Theoretical Development

II.1 Governing Equations

At the global level, the simulation of the deforming workpiece is based on balance of momentum, conservation of mass, and conservation of energy coupled with the appropriate kinematic and constitutive relations. The momentum and mass expressions are used to formulate the solution for the workpiece motion, while the energy equation is used to determine the temperature field. The focus of this paper is on the mechanical response, and although the thermal and mechanical responses often are tightly coupled, only the mechanical formulation need be discussed for our purpose here.

Balance of linear momentum, assuming no inertial terms and neglecting body forces, reduces to a vanishing stress divergence

$$\nabla \cdot \boldsymbol{\sigma} = 0 \tag{1}$$

The material characterization will neglect elasticity and retain only the isochoric plastic deformations of a fully dense workpiece. Conservation of mass then can be written for an incompressible motion as

$$\nabla \cdot \boldsymbol{u} = 0 \tag{2}$$

The numerical solution for the motion stems from the weak form of eqns (1) and (2). It may be cast in terms of a mixed formulation involving the velocity and pressure once the deviatoric stress is eliminated via a viscoplastic relationship of the general form

$$\boldsymbol{\sigma}' = \boldsymbol{C} \cdot \boldsymbol{D}' \tag{3}$$

Here, the velocity gradient $\boldsymbol{L}$ has been composed of a symmetric part $\boldsymbol{D}$ and a skew symmetric part $\boldsymbol{W}$. At a material point, the fourth order tensor $\boldsymbol{C}$ will be associated with a specific aggregate deemed to be underlying that point. As such, $\boldsymbol{C}$ will be a non-linear function of the orientations and slip system hardnesses for all crystals in the aggregate, as well as the deviatoric deformation rate $\boldsymbol{D}'$.

II.2 Constitutive Response

Situated in each element, at a computation point located at the element center, is a finite-sized aggregate of crystals. The aggregate is composed of crystals whose orientations are representative of the material as a whole. Each crystal in the aggregate is identified by Euler angles (φ, θ, ϕ) which specify orientation $g_c = (\varphi_c, \theta_c, \phi_c)$ with respect to a sample coordinate system. Crystal orientations g_c and associated volumes Δg_c are assigned such that the sum over all crystals in the aggregate approximates the integration of the orientation distribution function $\mathcal{F}$

$$\sum_c \mathcal{F}(g_c)\,\Delta g_c \approx \int \mathcal{F}(g)dg \tag{4}$$

Each orientation is then assigned a normalized weight w_c

$$w_c = \frac{\mathcal{F}(g_c)\,\Delta g_c}{\sum_c \mathcal{F}(g_c)\,\Delta g_c} \tag{5}$$

which dictates the contribution of this crystal to the aggregate response.

Crystals are taken to deform solely by crystallographic slip in which one plane of atoms shifts relative to others. First considering the deformation of any one crystal within an aggregate, we decompose its deformation gradient into that accommodated by slip through a stationary lattice, followed by rotation of the lattice (ASARO & NEEDLEMAN [1985])

$$\boldsymbol{F}^c = \boldsymbol{R}^* \boldsymbol{F}^p \tag{6}$$

This may be written in rate form in terms of the crystal velocity gradient and separated into symmetric and skew parts to give

$$\boldsymbol{D}^c = \boldsymbol{D}^p \tag{7}$$

$$\boldsymbol{W}^c = \dot{\boldsymbol{R}}^* \boldsymbol{R}^{*T} + \boldsymbol{W}^p \tag{8}$$

The crystal deformation rate and spin, respectively, may be related to the slip system shear rate

$$\boldsymbol{D}^c = \sum_\alpha \boldsymbol{P}^\alpha \dot{\gamma}^\alpha \tag{9}$$

$$\boldsymbol{W}^c = \sum_\alpha \boldsymbol{Q}^\alpha \dot{\gamma}^\alpha \tag{10}$$

where $\boldsymbol{P}^\alpha$ and $\boldsymbol{Q}^\alpha$ are the symmetric and skew portions of the Schmid tensor

$$\boldsymbol{T}^\alpha = \boldsymbol{\nu}^\alpha \otimes \boldsymbol{\eta}^\alpha = \boldsymbol{P}^\alpha + \boldsymbol{Q}^\alpha \tag{11}$$

Similarly, the resolved shear stress can be related to the microscopic (crystal) shear stress through the symmetric portion of the Schmid tensor

$$\tau^\alpha = \boldsymbol{P}^\alpha \cdot \boldsymbol{\sigma}'^c \tag{12}$$

At fixed state, the stress and the rate of shearing at the slip system level are coupled via the constitutive relation (HUTCHINSON [1976]; ASARO & NEEDLEMAN [1985])

$$\dot{\gamma}^\alpha = a\left(\frac{\tau^\alpha}{\hat{\tau}}\right)^{\frac{1}{m}} \tag{13}$$

where $\hat{\tau}$ is the slip system mechanical threshold. Here, all slip systems within a crystal are assumed to harden identically so a single variable fully describes the strength of the slip systems. Combining eqns (9), (12), and (13), the stress for a single crystal may be written in terms of the deformation crystal deformation rate and the stiffness, $\boldsymbol{C}^c$, as

$$\boldsymbol{\sigma}'^c = \boldsymbol{C}^c \cdot \boldsymbol{D}^c \tag{14}$$

where $\boldsymbol{C}^c$ is evaluated from inversion of

$$\boldsymbol{C}^{c-1} = \sum_\alpha a\left(\frac{\tau^\alpha}{\hat{\tau}}\right)^{\frac{1}{m}-1} \boldsymbol{P}^\alpha \otimes \boldsymbol{P}^\alpha \tag{15}$$

Eqn (14) must be solved for all crystals of an aggregate. The solution procedure is ideal for parallel processing because the equations are identical for all crystals and each solution is independent of the others.

Coupling of the sample and crystal level behavior is accomplished through the Taylor assumption: all crystals underlying a computation point experience the same deformation gradient. The Taylor assumption is used because we are modeling a FCC material taken to moderate strain, the rate sensitivity is low, more than 5 independent slip systems with comparable hardness are available, and there is at least a small degree of strain hardening. This microscopic/macroscopic link is achieved through the requirement that deformation be identical at the microscopic and macroscopic levels

$$\boldsymbol{F}^c = \boldsymbol{F} \tag{16}$$

or, equivalently, for the symmetric and skew portions of the velocity gradient

$$D^c = D \tag{17}$$

$$W^c = W \tag{18}$$

Eqns (16-18) satisfy compatibility at the microstructural level. However, equilibrium across crystals may not be satisfied.

Upon determination of the linearized constitutive behavior at the crystal level, it is necessary to combine responses of the individual crystals to give the macroscopic constitutive response. This is achieved by forming the weighted average of the crystal level constitutive matrices

$$C = \sum_c w_c C^c \tag{19}$$

resulting the the macroscopic constitutive relation given in eqn (3).

In the following work we consider the uniaxial compression of a cylindrical specimen composed of material exhibiting orthorhombic symmetry. This specimen symmetry enables the modeling of one-quarter of the specimen. It is necessary that the stress state resulting from the Taylor model assumptions described above be consistent with the boundary conditions posed for this problem. To this end, we require that the shear stress components σ'_{12}, σ'_{23}, and σ'_{13} vanish (or are at least be very small) when these components are recovered using the coaxial $\boldsymbol{D}'$ used to develop $\boldsymbol{C}$ according to eqns (4), (5), and (19). This requirement can only be satisfied through the specification of the crystal orientations in the aggregate underlying a computation point. In this work, two alternative means of enforcing this requirement are explored:

1. exactly, at the computation point level by explicit application of orthorhombic symmetry operations to crystals composing the aggregate;

2. in an average, macroscopic sense by forming spatially distinct aggregates using different samples of crystal orientations with associated weights which approximately integrate the orientation distribution, and with sampling sufficient to approximate orthotropic response in the global system of equations.

In Appendix B, it is shown that the application of orthorhombic symmetry operations leads the the development of an orthotropic constitutive matrix.

The latter option of generating aggregates with different distributions, having some deviation from orthotropy, is discussed in the initialization of state.

To this point only the response of crystals or aggregates of crystals at fixed state has been discussed. As deformation occurs, the material microstructure changes and the state variables must evolve to reflect these changes. For the polycrystalline models the crystal may both reorient and harden. The evolution equation for the reorientation stems from the kinematics at the crystal level. The rate of change in the rotation of a crystal from its original to current orientation may be written

$$\dot{\boldsymbol{R}}^* = (\boldsymbol{W}^c - \boldsymbol{W}^p)\boldsymbol{R}^* \tag{20}$$

while for the hardening, the rate of change of the mechanical threshold is given in general terms as

$$\dot{\hat{\tau}} = H(\hat{\tau}, |\dot{\gamma}|)|\dot{\gamma}| \tag{21}$$

The detailed form of $H(\hat{\tau})$ is discussed by MATHUR & DAWSON [1989].

III Data Parallel Implementation

As indicated in the introduction, parallel processing opportunities exist at several levels in the simulation of the deformation of materials. At the global level in an implicit formulation, the finite element discretization involves the formation of element matrices, the assembly of the elemental contributions into the global matrix equation, and finally the solution of the matrix equation. The first two of these are easily accomplished within a parallel computing environment, while the third has been more difficult to accomplish with efficiency. Iterative solvers generally are better suited for a parallel environment, and have been successfully used in formulations for elasticity (MATHUR & JOHNSSON [1989]) and compressible fluid flow (JOHAN *et al.* [1991]). However, within the context of plasticity formulations, the incompressibility constraint has proved difficult to enforce while ensuring convergence of the iterative algorithm.

Further opportunity for parallel computation lies at the computational point level. That is, for materials comprised of an underlying microstructure whose elements dictate the mechanical response, an aggregate of elements must be examined at integration stations within the finite element formulation to determine the material constitutive response. For polycrystalline metals acting under the Taylor hypothesis, the microstructural calculations for the stress and crystal reorientations are essentially independent and may be performed easily in parallel. Further, as the population of crystals is very large when the product of the aggregate size and the number of computation points is considered, the potential benefit for performing the calculations in parallel is great.

The simulations discussed herein embody all of the parallel structures mentioned in the preceding two paragraphs. Unique in this work are the efforts to take advantage of massively parallel computer architecture for the crystal level calculations and the iterative solution of the global matrix equation. Each of these will be discussed in more detail in the remainder of this section.

III.1 Data Parallel Algorithm for Crystal Equations

In considering the numerical implementation of this simulation on a massively parallel computer, it is convenient to think of all crystals of a workpiece as being arranged in a rectangular array with each row containing of all the crystals of one aggregate (Figure 1). There are as many columns in the array as there are crystals in each aggregate and as many rows as aggregates within the workpiece. This arrangement has a one-to-one correspondence with the algorithms used to map arrays in the parallel architecture (THINKING MACHINES INC. [1991]).

At the macroscopic level a unique value of stress must be derived from all the crystals in a row of the array. Thus, from the perspective of a deformation-driven calculation, the macroscopic velocity gradient must be "broadcast" to each crystal of an aggregate for use within the calculations of crystal stress and crystal reorientation. The macroscopic stress is a consequence of averaging crystal stresses across a row in the array. As each material point at the macroscopic level potentially has a unique velocity gradient, each row in the array receives different "data" for crystal computations.

The specific steps of the calculations at the crystal level, which might be executed either to evaluate the crystal contribution to the material stiffness matrix $[C]$ or to update the Euler angles $(\psi_c, \theta_c, \phi_c)$, are listed below.

1. The macroscopic velocity gradients, evaluated for each aggregate (or element), are broadcast across processors to all crystals of all aggregates.

2. A sequence of data parallel operations are performed in which:

   (a) the macroscopic deformation rate first is rotated to the crystal coordinate system

   (b) the crystal stress then is evaluated using the non-linear constitutive behavior appropriate for crystallographic slip, which is followed by either

      i. computing the effective, linearized, constitutive matrix in the macroscopic reference frame, or

      ii. updating the orientation of crystals

3. Weighted averages of all constitutive matrices are computed to give the effective bulk macroscopic constitutive matrices to be used in the finite element computation.

In the context of the data layout described above, the broadcast operation is like spreading a vector of dimension equal to the number of rows (aggregates) to all columns. The broadcast of data to all crystals and the averaging of crystal responses to derive macroscopic properties involve native Connection Machine operations.

III.2 Finite Element Formulation and Iterative Solution Procedure

Following the notation of HUGHES [1987], the finite element formulation is developed from the weak forms of the equilibrium statement (1)

$$a(\boldsymbol{v},\boldsymbol{u}) - b(\boldsymbol{v},\boldsymbol{u}) = (\boldsymbol{v},\boldsymbol{f}) + (\boldsymbol{v},\boldsymbol{t})_\Gamma \tag{22}$$

and the mass conservation statement (2)

$$(v, \nabla \cdot \boldsymbol{u}) = 0 \tag{23}$$

Upon introduction of appropriate weight functions and linearization of the constitutive response, finite element procedures lead to the discretized system of equations (THOMPSON [1969]; ZIENKEWICZ [1977])

$$\begin{bmatrix} K_D & -G \\ -G^T & 0 \end{bmatrix} \begin{Bmatrix} U \\ P \end{Bmatrix} = \begin{Bmatrix} f \\ 0 \end{Bmatrix} \tag{24}$$

In a parallel computing environment it is customary to use an iterative procedure, such as the conjugate gradient method, to solve the system of equations (24). However, two significant complications arise in the viscoplastic formulation. Owing to the non-linear dependence of the the matrix $[K_D]$ on the velocity field, the linearized form (24) must be repeatedly solved to develop the constitutive response (DAWSON [1984]). The incompressibility constraint introduces a further complication in that it degrades the condition of the eqns (24). This leads to a prohibitive number of conjugate gradient iterations in the development of the velocity field. It is customary when using the

conjugate gradient method to perform operations on the coefficient matrix to improve its conditioning and consequently enhance numerical performance. In this discussion the preconditioning is limited to diagonal scaling.

In the following formulation, we seek to further decouple the incompressibility constraint from the conjugate gradient procedure. To develop a penalty method, it is general practice to introduce a "constitutive" relationship

$$p = -\beta \nabla \cdot \boldsymbol{u} \tag{25}$$

where β represents the bulk viscosity for a slightly compressible fluid. The parameter β is chosen in some manner which balances maintenance of the incompressibility constraint with numerical performance. In preparation for an iterative procedure, and following ZIENKEWICZ *et al.* [1985], an alternative constraint

$$-\lambda \nabla \cdot \boldsymbol{u}^{i+1} = p^{i+1} - p^i \tag{26}$$

is posed. This is a statement that convergence of the pressure in the $i+1$ iterate assures an incompressible velocity field $\boldsymbol{u}_{i+1}$. Upon introducing (26) into the weak forms (22) and (23), finite element procedures lead to the discretized system of equations

$$\left[K_D + \lambda G M^{-1} G^T\right] \{U^{i+1}\} = \{f\} + [G]\{P^i\} \tag{27}$$

and

$$\{P^{i+1}\} = \{P^i\} - \lambda [M]^{-1} [G]^T \{U^{i+1}\} \tag{28}$$

where $[M]$ is taken to be the pressure mass matrix of the Consistent Penalty Method presented by ENGELMAN *et al.* [1982]. Equation (27) is solved (also in iterative fashion) by the conjugate gradient method. Upon determination of the velocity, the pressure is updated using (28). Use of piecewise discontinuous shape functions for the pressure field enables the construction and inversion of $[M]$ at the elemental level. This allows for a data parallel development of the elemental matrices $[K_D]$, $[G]$, and $[M]^{-1}$. Details of gathering elemental matrices for solution of the global system of equations is given by MATHUR *et al.* [1992].

The key factor in this approach is that the penalty parameter λ need not necessarily be large. As such, the linear system remains well-conditioned in the early iterations of eqns (27) and (28). This effectively decouples the conjugate gradient solution for the velocity in eqn (27) from the incompressibility

constraint for these initial iterations. Numerical difficulties inherent in the velocity-pressure formulation appear only in excessive iterative attempts for which the previous iterate $\{U^i\}$ has converged to the correct solution within acceptable numerical precision. This yields a convergent iterative algorithm and enables the effective use of a parallel environment.

Additional benefits can be derived from this iterative procedure when material properties are a non-linear function of the deformation rate (ZIENKEWICZ *et al.* [1985]). The kinematic dependence of the stiffness matrix $[K_D]$ is updated at each iteration of eqn (27) based on the previous velocity field $\{U^i\}$. However, the material state as characterized by the weighted orientations and slip system hardnesses is not updated in the course of these iterations.

A simple Euler update is used to update the problem geometry. The geometry is advanced using the converged solution from the iterative procedure just described. The material state is correspondingly updated using the data parallel algorithm detailed above. The deformation is performed with a variable time step, with finer time steps taken in the initial iterations.

IV Materials and Method

IV.1 Mechanical Testing

Cylindrical specimens were machined from hot rolled 3000 series aluminum alloy plate with the axis in the normal direction (ND). This stock was chosen as it was available with dimensions sufficient to machine into compression specimens. The specimens were then deformed at a constant true strain rate of 1 s^{-1} using closed loop control on a servo-hydraulic load frame.

Undeformed and deformed specimens are shown in Figure 2. During compression the circular cross-section became oval, with the long cross-sectional axis corresponding to the original rolling direction and short axis to the transverse direction. This indicates that principal directions of the compression deformation were coincident with the axes of material symmetry established by rolling, as detailed in the texture analysis discussion below.

IV.2 Texture Analysis

Samples for x-ray analysis were prepared from both undeformed stock and deformed specimens. The sample orientation was taken with the normal coincident with normal direction of the rolling process. Pole figures ({111}, {200}, and {220}) were obtained using a 4-circle pole figure goniometer. The x-ray data was analyzed using the popLA ("preferred orientation package - Los Alamos") software (KALLEND *et al.* [1991]). Several operations were performed which:

1. rotated the pole figures about the normal axis to remove sample alignment errors;
2. normalized the pole figures and completed the periphery of each figure using harmonic analysis (BUNGE & ESLING [1985]); and
3. developed the sample orientation distribution, or SOD (WENK & KOCKS [1987]), using the WIMV method (MATTHIES & WENK [1985]).

The normalized, completed pole figures of the experimental data collected on the undeformed specimen are shown in Figure 3A.

Quantitative analysis of these pole figures leading to a mathematical description in the form of an orientation distribution function requires that some judgement be made as to the sample symmetry inherent in the material. The qualitative appearance of the pole figures in Figure 3A suggests the presence of orthorhombic sample symmetry. This is also in agreement with the pole figure data being derived from the center plane of rolled stock. Analysis was thus performed using the WIMV algorithm with implied orthorhombic symmetry. The effects of this choice on the boundary value problem studied in this work will be discussed subsequently in detail.

Pole figures recomputed as part of the WIMV algorithm are shown in Figure 3B. Orthorhombic symmetry is clearly evident. The WIMV algorithm converged quite rapidly for this experimental texture data. The value of the RMS relative error averaged over the pole figures was 2.9% after 6 iterations (KALLEND *et al.* [1991]).

The popLA software also can generate pole figures and orientation distributions from the discrete data through the DIscrete ORientation program (DIOR). This program was used in the following work to generate the graphical results from the weighted, discrete orientations used in the simulations.

IV.3 Initialization of State

IV.3.1 Explicit specification of orthotropy at the aggregate level

To utilize the finite element code for material with initial anisotropy, it is necessary to characterize the initial material state. The polycrystalline approach may be considered to be a state variable approach with the number of state variables equaling the number of crystals in an aggregate times the number of identifying variables within a crystal. For example, if the material state is described by 256 crystals, each of which has an orientation specified by 3 Euler angles and a strength, the number of state variables totals 1024. However, it may be advantageous to weight each crystal's contribution to the averaged aggregate properties differently. To do this a weight parameter, whose value remains fixed throughout the course of a deformation, is assigned to each crystal. In this case, the 256 weights and 768 Euler angles must be selected together so that resulting density distribution accurately represents the texture observed in an x-ray analysis.

The WEIGHTS program of the popLA package was utilized to derive a weighted set of 256 discrete Euler angle locations from the sample orientation distribution (KOCKS [1990]). Symmetry operations required for orthorhombic sample symmetry were then applied to the 256 locations resulting in a distribution of 1024 weighted discrete orientations to be used in the simulation. Every finite element was assigned an aggregate with this identical distribution of state parameters.

Pole figures reconstructed from this weighted set of orientations are shown in Figure 3C. The orthorhombic symmetry present in this discretized representation of the texture is readily apparent.

IV.3.2 Random sampling of the sample orientation distribution

In this approach, the orthotropic material response is not satisfied locally. However, sufficient symmetry is present to satisfy the imposed boundary conditions when the average response is considered over all elements. In other words, orthotropy is achieved in a macroscopic sense by element contributions to the global stiffness matrix.

An aggregate is situated in each finite element. However, in contrast to the approach described in the previous subsection, each aggregate contains a distinct set of crystals. Random sampling is performed to develop a different set of orientations for each aggregate. Three independent identically distributed random variables Ψ, Θ, and Φ which follow a uniform distribution are defined. Also defined is an integer random variable specifying an orthorhombic symmetry operation (Appendix B)

$$\Pr(O = 1) = \Pr(O = 2) = \Pr(O = 3) = \Pr(O = 4) = \frac{1}{4} \qquad (29)$$

The orientation distribution generated by WIMV is in a discretized form. Densities are listed on a $5° \times 5° \times 5°$ mesh. To generate a weighted orientation, or a crystal in the aggregate, a sample is taken of the above random variables. The Euler angles are used to evaluate the crystal's weight from the density created by the WIMV algorithm through linear interpolation of the discretized orientation distribution. A sample symmetry rotation is conducted as specified by the random value of the symmetry parameter, O.

This procedure is performed for all crystals in a parallel fashion. An array structure with dimensions of the number of elements by number of

crystals in an aggregate is initialized with random values by a single call to the native data parallel random number generator. Interpolation and rotation are the performed concurrently. Pole figures reconstructed from 1024 weighted orientations developed using this random sampling technique are shown in Figure 3D.

Slip system model parameters were developed to approximate the channel die compression of aluminum. The values used in this work were $\dot{a} = 1.0$, $m = 0.05$, and, $\hat{\tau}_i = 27.2$ (for all slip systems).

V Results

The compression of specimens to one-half of the original height was simulated to correspond to the experiments described earlier. The problem geometry was discretized into 256 elements using 8-node brick elements. The deformation was carried out in 50 time steps. Simulations were repeated for several different methods of defining the aggregates of crystals within the finite elements. First, simulations were performed using a weighted discrete orientation file created by the WEIGHTS program of popLA. In the following discussion, the results for these simulations are labeled "WTS". Simulations also were performed in which the element aggregates were defined using the random sampling procedure with crystal to aggregate ratios of 1024, 256, 64, and 16. These simulations are denoted by the crystal to aggregate ratio. Multiple simulations were made for each crystal to aggregate ratio.

The weighting factors for crystals were chosen from the orientation data for the rolled specimens prior to compression. However, to verify the soundness of the random sampling technique, simulations first were carried out based on aggregates chosen from a uniform density orientation distribution. The results of these simulations yielded the expected result that an untextured circular cylindrical specimen retained a circular cross-section. The deformations were essentially axisymmetric, with no preferred directions within the plane having its normal in the compression direction.

V.1 Predictions of Specimen Deformation

As stated previously, a predominantly coaxial deformation mode is developed in the experimental specimens, where by coaxial it is meant that the principal axes of the deformation align with those of the principal symmetry axes of the initial material. Deformed meshes for the WTS simulation and the random sampling (64 crystals per aggregate) are shown in Figure 4. In the WTS simulation, every aggregate was initially identical with orthotropy enforced at the aggregate level. As a consequence, a very uniform deformation behavior was achieved (Figure 4A). To the numerical precision held in the simulations, there was no gradient in the velocity along the specimen cylindrical axis.

Results from the random sampling simulations demonstrated a dependence of deformation pattern on number of crystals per aggregate. Simula-

Method	Ovaling	
WTS	1.166	
1024	1.129	$(n = 2)$
256	1.134	$(n = 2)$
64	1.132	$(n = 3)$
16	1.132	$(n = 4)$
Experimental	1.103 ± 0.005	$(n = 8)$

Table 1: Average ratio of long cross-section axis to short cross-section axis based on n trials

tions conducted with 1024 crystal to aggregate ratio were very similar to the WTS simulation with little variation in velocity along the specimen axis and minimal shearing between elements. The variation of cross-sectional velocity components along the cylindrical axis was less than 0.5%. As the crystal to aggregate ratio decreased, localized shearing was observable in elements. This shearing is evident in Figure 4B. All of the simulations overpredicted the actual specimen ovaling (Table 1).

To better characterize the localized variations in deformation, the average and standard deviation of the velocity gradient components were examined for each crystal to aggregate ratio. These values were developed by averaging the velocity gradient for all elements (Table 2). Averaging was performed after the first converged solution for the onset of deformation and prior to any update of the specimen geometry. For all cases the averaged off-diagonal components are small when compared with the diagonal components. On the average, or considering a geometric volume scale on the order of the specimen size, deformation is coaxial. However, the standard deviation of the components increases with decreasing crystal to aggregate ratio. This indicates that locally, at the geometric scale of an element volume, there exists an increasing variation of the shear components of the deformation throughout the specimen with decreasing crystal to aggregate ratio.

1024	0.526 ± 0.003	0.000 ± 0.004	0.000 ± 0.002
	-0.000 ± 0.005	0.474 ± 0.003	-0.000 ± 0.002
	-0.000 ± 0.002	0.000 ± 0.002	-1.000 ± 0.002
256	0.538 ± 0.007	0.001 ± 0.013	-0.002 ± 0.005
	-0.001 ± 0.012	0.462 ± 0.008	-0.003 ± 0.005
	0.001 ± 0.005	0.001 ± 0.005	-1.000 ± 0.010
64	0.539 ± 0.012	-0.001 ± 0.029	-0.001 ± 0.009
	-0.002 ± 0.024	0.461 ± 0.011	-0.000 ± 0.008
	0.001 ± 0.011	0.003 ± 0.011	-1.000 ± 0.008
16	0.541 ± 0.030	-0.010 ± 0.055	-0.002 ± 0.019
	0.000 ± 0.056	0.459 ± 0.028	0.004 ± 0.022
	0.002 ± 0.030	-0.005 ± 0.023	-1.000 ± 0.017

Table 2: Mean and standard deviation of components of elemental velocity gradients

V.2 Texture Predictions

Textures following compressive deformation from selected simulations are shown as polar sections of the crystallite orientation distribution (COD) in Figure 5. These are constant o sections in Euler space using that when overlaid yield the projection of the {100} pole figure [1987]. Also shown is the COD section plot developed from the WIMV analysis of a deformed specimen. The DIOR program was used to construct the COD sections produced by the numerical simulations. In all cases, 1024 discrete weighted orientations were used as input. The COD for the 1024 crystal to aggregate ratio case draws crystals from only a single element. At the other extreme, the 16 crystal to aggregate ratio case requires use of 64 elements to create the COD sections. Orthorhombic sample symmetry operations and cubic crystal operations were applied to each discrete location to develop equivalent orientations in an Euler space volume of $\frac{\pi}{2} \times \frac{\pi}{2} \times \frac{\pi}{2}$. The sections were plotted using a logarithmic scale, retaining an identical scale for all sections. This casts the results in a rather harsh light, but enables critical comparison.

Results for the WTS simulation show that some components in the experimental texture are omitted. Other components of the WTS texture are of much greater density than found in the experiment. In particular, there

exists a position of elevated density along the specimen 2 axis (transverse direction) present on the $\phi = 0°$ and $\phi = 90°$ COD sections. This texture component is denoted by an arrow in Figure 5.

For the random sampling, all of the pre-dominant components of the texture are present. However, the 1024 crystal to aggregate case shares the elevated density along the specimen 2 axis (again denoted by an arrow). This artifact gradually decreases with decreasing crystal to aggregate ratio. All simulations lack some of the background present in the experimental texture. Most notable is the diffuse component of texture at the origin present in all COD sections of the experimental results. With the scale adopted in these plots, only the 16 crystal to aggregate ratio simulation exhibits such texture components, and then only on the $\phi = 20°$ and $\phi = 40°$ COD sections.

Further insight is gained by comparing the quarter pole figures shown in Figure 6. These pole figures are the {100} projections from the orientation sections of Figure 5 plotted with a scale which more appropriate for this projection. The peak texture component in the experimental pole figure is similar in magnitude and location to the 256 and 64 crystal to aggregate ratio simulations. The corresponding location in the 16 crystal to aggregate ratio case is of less intensity. In contrast, only the 16 crystal to aggregate ratio pole figure exhibits a component of texture coincident with the specimen normal direction at the pole figure center (lower-left hand of section). This texture component is readily observable in the experimental pole figure.

VI Discussion

The simulations with randomly selected populations of crystals illustrate a number of important issues relative to modeling the mechanical response of polycrystalline materials. The essential feature of random sampling, which is performed independently for each of the aggregates within the workpiece, is that it introduces some degree of spatial variability in the mechanical properties. This variability tends to decrease as the ratio of crystals to aggregate increases.

In the limit of a very large crystal to aggregate ratio, the sampling of each aggregate is sufficient to ensure that all aggregates display the properties expected for the complete orientation distribution. Properties are essentially homogeneous for spatial locations derived from a common orientation distribution. At the other extreme is the selection of a small number of crystals to represent an aggregate. The "aggregate" then may be interpreted as representing the interaction between a collection of nearest neighbor crystals as governed by a microstructural model (in this work the Taylor model). A possible choice for a lower limit is based on the space-filling model advanced by LORD KELVIN [1887]. In this case, each crystal is represented by a tetrakaidecahedron with 14 faces, each in contact with a nearest neighbor. We choose as a minimum representation an aggregate consisting of 16 neighboring crystals, simply because a power of two leads to better use of the parallel architecture. Interaction between aggregates is achieved at a global level by satisfaction of the equilibrium and continuity requirements inherent in the finite element formulation.

In contrast, when the same sample of crystals defines the aggregate initially at all spatial locations within the workpiece, the properties are homogeneous. This is true regardless of how the sample was chosen and whether or not it replicates the behavior of the full orientation distribution well. In this work, the WTS aggregates were chosen to reproduce the initial texture to the greatest extent possible with a limited number of crystals. Indeed, compared to aggregates with equivalent numbers of randomly sampled crystal orientations, the WTS file will better represent the orientation distribution (KOCKS *et al.* [1990]). The important difference to keep in mind, however, is that with the WTS representation, exactly the same aggregate is used at every spatial location in the workpiece; while with the randomly sampled ag-

gregates, the various aggregates within the workpiece differ from each other.

The impact of spatially varying properties is profound. There is a distinct coupling between the existence of variable properties and the evolution of texture. Consequently, as the deformation proceeds the texture development in a workpiece with inhomogeneous properties may be quite different from one with initially uniform properties. As opposed to situations where the surface velocities of the workpiece are fully prescribed, this is more pronounced for applications having traction-free boundaries. Specification of kinematic boundary conditions requires that the average component values of the velocity gradient are predetermined, irrespective of local inhomogeneities in deformation field. In the case of traction-free boundaries, there is a mutual dependence between the deformed geometry and the texture evolution: altering texture evolution implies a different strain path.

The existence of spatially varying properties causes the body to respond differently to external loading than if the properties are uniform. This is evident in the comparison of the velocity gradients given in Table 2. While the average macroscopic deformations are consistent with a coaxial deformation and at the macroscopic level equilibrium is satisfied, internally the deformation varies more as the crystal to aggregate ratio decreases. For the compressive loading case examined, the variability in velocity gradient implies the existence of shearing components of the deformation gradient. Individual aggregates thus experience different strain paths with the result that for neighboring aggregates the texture evolution is not the same. The variation in the deformation rate retards the texture evolution in comparison to that in a workpiece with uniform properties. This decrease in the rate of texture evolution is clearly evident in the pole figures generated by the 16 crystal to aggregate ratio simulation when compared to both experimental data and simulations with higher crystal to aggregate ratio (Figure 5).

It has long been known that polycrystalline models based on the Taylor hypothesis of equal straining of all crystals texture too quickly (DILLAMORE & KATOH [1974]). This has been attributed to the inability of the model to account for local inhomogeneities in deformation as well as the limited manner in which crystal interactions occur. Such shortcomings have spawned investigations of models which enforce combinations of equilibrium and compatibility differently from the Taylor hypothesis. In this work, the Taylor hypothesis has been retained for the response of every aggregate.

but not globally. Through the finite element discretization of the workpiece interactions of distinct aggregates occur through the global system of equations. No specific action was taken to damp the rotation of a specific crystal: textures are more diffuse because of the variation in velocity gradient from aggregate to aggregate. It is of note that, in the specific case of 16 crystals in an aggregate, a texture computed using the Taylor model exhibits retarded development when compared to experimental texture measurements.

For small crystal to aggregate ratios, it may be useful to think of the aggregates as small clusters of crystals that act as a unit to define the properties of a computation point at the macroscopic scale. Because of finite crystal size, it is not reasonable to allow the number of crystals in a single cluster to become large enough to represent the full orientation distribution well. Rather, the deformation is not uniform over spatial dimensions containing a population of crystals sufficient to characterize the orientation distribution. By considering small clusters of crystals with the attribute that each cluster is chosen at random independently of others, real spatial variability of properties can be simulated.

Interaction between the macroscopic and microscopic aspects of polycrystalline simulations are not limited to the issue of spatial variability from aggregate to aggregate. Macroscopic and microscopic coupling extends to the interplay between boundary conditions posed in the plasticity problem and the degree of material symmetry inherent in the problem domain. Without accounting for material symmetry through specification of Euler angles in aggregate(s), a very different deformation may be developed than would be expected. To our knowledge, this issue is little addressed in previous finite element modeling efforts using polycrystalline theory. One study that did address this issue is that of HARREN & ASARO [1989], who achieved a globally orthotropic deformation through the development of an orthotropic unit cell consisting of crystals with idealized two-dimensional slip systems.

There are perhaps two reasons for the limited treatment of material symmetry in macroscopic deformation problems. Many simulations have used an initially uniform specification of orientations (MATHUR & DAWSON [1989]; BRONKHORST *et al.* [1991]; KALIDINDI *et al.* [1991]). With adequate sampling of crystals in the aggregate, such that on the order of hundreds of crystals contribute to the representation of the deformed texture, material symmetry is naturally developed through the course of the deformation.

Another possible reason is the problems that have been studied are predominantly plane strain compression simulations such as rolling, wire drawing, or channel die compression (HARREN & ASARO [1989]; MATHUR & DAWSON [1989]; BECKER [1991]). Here the spatial kinematics are dominated by the strict enforcement of kinematic boundary conditions. A longer term goal for using polycrystalline plasticity theory must be for simulating sheet metal forming processes such as deep drawing. Here, the interplay between initialization of texture, material symmetry, and boundary conditions will be in the forefront of the modeling effort.

We selected to model only a quarter of the cylindrical specimen with planar boundaries aligned with the axes of material symmetry. This choice is consistent with the decision, based on experimental texture measurement, to represent the texture with a $\frac{\pi}{2} \times \frac{\pi}{2} \times \frac{\pi}{2}$ section of Euler space. This consistency is explicitly maintained in the WTS simulations where each aggregate represents a uniformly orthotropic material. As a consequence, normal tractions are not developed on the symmetric faces of the quarter cylinder. Such will not be the case when the aggregates are formed by random sampling of the sample orientation distribution. In this case the symmetry of the deformation is preserved, but non-zero tractions will be present along the planes of symmetry. This is a macroscopic effect of applying the Taylor model with spatially distinct aggregates only partially representative of the orientation distribution. Similar trade-offs to those made in the development of microstructural models apply in the application of these models at a macroscopic scale. In our application, much is gained by analyzing the experimental data with a maximum of symmetry. The specification of the macroscopic boundary value problem should be consistent with the analytic description of the texture. Specific microstructural choices are reflected in the macroscopic solution.

This work is similar in spirit to investigations of nonuniform deformation developed through discretization at the microstructural level (HARREN & ASARO [1989]; BECKER [1991]; KALIDINDI *et al.* [1991]). In these studies the individual crystals are discretized and continuity between crystals is achieved through the finite element formulation. Interaction between neighboring crystals leads to locally nonuniform deformation with a concomitant modification on the prediction of texture development. The texture resulting from the finite element treatment of the microstructure may differ sig-

nificantly from that predicted using the Taylor theory, both in the rate of texturing and the absence or presence of texture components.

In contrast to these microstructural studies (HARREN & ASARO [1989]; BECKER [1991]; KALIDINDI *et al.* [1991]), the current work treats material inhomogeneities on a macroscopic scale. It is still necessary to adopt a microstructural model from which to derive the constitutive response at a computational point (here the choice happens to be the Taylor assumption). However, with aggregate to aggregate variability the deformation is not homogeneous on a scale spanning different elements (or quadrature points). Thus it is the spatially heterogeneous properties arising from the small sample size that gives rise to inhomogeneous deformation, without need to abandon the microstructural theory deemed appropriate for a given application. Such variability can't be obtained directly if the same aggregate, regardless of size, is assigned to each spatial point in a workpiece. Further, retaining the approach of an aggregate of crystals which act in accordance to some microstructural model enables the initialization of texture on a macroscopic scale.

This work does not intend to displace efforts in the development of microstructural models. Indeed, self-consistent (HUTCHINSON [1976]; MOLINARI *et al.* [1987]) or relaxed constraint models (HONNEFF & MECKING [1975]) may lead to much improved results. Our results simply suggest that spatial inhomogeneities also play a role in the texture evolution. On a more algorithmic note, these models may provide interesting challenges in a parallel implementation. Crystal interactions must be translated into interprocessor communication; such communication is minimal when using the Taylor model.

It is often said of the finite element method that the real effort, in terms of man-hours, lies in mesh preparation. Much the same can be said of the initialization of texture in this work. We found our results to be sensitive to the initial texture measurements. Several sets of pole figures and the orientation distributions were developed. X-ray technique plays a large part in the accuracy of the resulting orientation distribution. Visual comparison of pole figures from different experimental tests may compare very favorably in a qualitative sense. However, the quantitative orientation distributions derived from analysis of different sets of pole figures led to significant variations of deformational behavior in the numerical simulations.

# of elements	= 256	
# of nodes	= 387	
# of dof	= 1161	
# of aggregates	= 256	
Crystal to aggregate ratio	= 256	512
# of time steps	= 50	
Total simulation time	= 1426 s	2525 s
Time per element per crystal per time step	= 0.44 ms	0.38 ms

Table 3: Timing statistics for simulation conducted on an 8K CM-2 configuration

The numerical simulations represent the solution of an initial value problem with thousands of initial values in the form of weighted crystal orientations and slip system hardnesses. Clearly, the quality of the numerical predictions is constrained by the quality of the input. We carried out several WTS simulations using weighted orientations derived from different sets of experimental pole figures. The predictions of specimen ovaling improved with the quality of the pole figure data collected on the four circle goniometer. This leads to the conclusion that experimental issues such as goniometer alignment, correction for defocusing and background, and pole figure normalization play a large role in specifying the initial conditions which lead to correct prediction of specimen deformation.

The simulations described in this work are computationally expensive. The computational demands of simulations of plastic deformation based on polycrystalline plasticity theory has been documented in the literature (SMELSER & BECKER [1991]). Extending the application of theory from plane strain applications to more general three-dimensional deformation problems furthers the requirements made of both software and hardware. Modern parallel processing architectures enable these simulations to be conducted in timely fashion. Execution time statistics for simulations with crystal to aggregate ratios of 256 and 512 are listed in Table 3. Simulations using 1024 crystals per aggregate required a minimum 16 K processor CM-2 configura-

tion. In contrast, convergence of the conjugate gradient method for the lower crystal to aggregate ratio cases was slower as a consequence of the locally more inhomogeneous deformation field. Parametric studies, such as the effect of crystal to aggregate ratio on the development of texture, are clearly manageable with present architectures.

The combination of polycrystalline theory and modern parallel processing provides a powerful tool for the analysis of inelastic deformation for a large class of engineering materials. The successful application of polycrystalline theory rests on a history of fruitful developments in quantitative texture analysis (BUNGE [1982]; BUNGE & ESLING [1985]; MATTHIES & WENK [1985]). Through this theory, we may make a quantitative measurement of the state of our material. In addition, the theory enables one to represent this state by specifying the orientation of thousands of crystals which represent a sample of, or aggregate contained in, the material. Massive parallel processors then allow for the effective computation of the material response derived from the aggregate response based on the action of individual crystals. The beneficial interaction of theory and computational horsepower extends beyond the details of simulation. A consequence of massive parallel computations is the need to view and interpret tremendous quantities of data in a manageable fashion. In these polycrystalline based simulations, this need is met by theory to develop the orientation distribution function and graphical tools for display of the orientation distribution already in place (WENK & KOCKS [1987]). The blend of theory and massive parallel processing now enables one to study the development of texture in three-dimensional spatial problems of engineering interest.

Acknowledgements

This work was supported through Office of Naval Research contract N000 14-90-J-1810. Access to computing resources was provided by the Advanced Computing Laboratory at Los Alamos National Laboratories, the Pittsburgh Supercomputing Center, and the Connection Machine Network Server Pilot Facility of Thinking Machines, Inc.. Frequent interactions with Fred Kocks, both in the use of the popLA software package and the discussion of our research efforts, contributed much to this work. Maura Weathers, of the Materials Science Center at Cornell University, provided much assistance in the experimental pole figure measurement.

References

[1887] KELVIN, Lord (THOMPSON W.) "On the Division of Space with Minimum Partitional Area." *Philos. Mag.* **24**, 503.

[1938] TAYLOR, G.I., "Plastic Strain in Metals." *J. Inst. Metals* **62**, 307.

[1969] THOMPSON, E.G., MACK, L.R., and LIN, F.-S., "Finite Element Method for Incompressible Slow Viscous Flow with a Free Surface." *Dev. Mech.* **5**, 93.

[1974] DILLAMORE, I.L. and KATOH, H., "A Comparison of Observed and Predicted Deformation Textures In Cubic Metals." *J. Metal Sci.* **8**, 21.

[1975] HONNEFF, H. and MECKING, H., "Influence of the Geometry of the Deformation on the Rolling Texture of F.C.C. Metals," in DAVIES, G.J., DILLAMORE, I.L., HUDD, R.C. and KALLEND, J.S. (eds.), *Texture and the Properties of Materials*, Proceedings of ICOTOM V, Springer, Berlin, p. 265.

[1976] HUTCHINSON, J.W., "Bounds and Self-consistent Estimates for Creep of Polycrystalline Metals and Composites," *Proc. Roy. Soc. London A* **348**, 101.

[1976] VANHOUTTE, P. and AERNOUDT, E., "Considerations of the Crystal and the Strain Symmetry in the Calculation of Deformation Textures with the Taylor Theory," *Mater. Sci. Eng.* **23**, 11.

[1977] ZIENKEWICZ, O.C., "The Finite Element Method," 3rd. ed., McGraw-Hill, London.

[1982] BUNGE, H.J., "Texture Analysis in Materials Science," Butterworths, London.

[1982] ENGELMAN, M.S., SANI, R.L., GRESHO, P.M., and BERCOVIER, M., "Consistent vs. Reduced Integration Penalty Methods for Incompressible Media Using Several Old and New Elements," *Int. J. Num. Meth. Fluids* **2**, 25.

[1984] DAWSON, P.R., "A Model for the Hot or Warm Forming of Metals with Special Used of Deformation Mechanism Maps," *Int. J. Mech. Sci.* **26**, 227.

[1985] ASARO, R.J. and NEEDLEMAN, A., "Texture Development and Strain Hardening in Rate Dependent Polycrystals," *Acta Metall.* **33**, 923.

[1985] BUNGE, H.J. and ESLING, C., "The Harmonic Method," in WENK, H.-R. (ed.), Preferred Orientation in Deformed Metals and Rocks: An Introduction to Modern Texture Analysis Academic Press Inc., Orlando, pp. 109-122.

[1985] MATTHIES, S., WENK, H.-R., "ODF Reproduction with Conditional Ghost Correction," in WENK, H.-R. (ed.), Preferred Orientation in Deformed Metals and Rocks: An Introduction to Modern Texture Analysis Academic Press Inc., Orlando, pp. 139-147.

[1985] WENK, H.-R., "Measurement of Pole Figures," in WENK, H.-R. (ed.), Preferred Orientation in Deformed Metals and Rocks: An Introduction to Modern Texture Analysis Academic Press Inc., Orlando, pp. 11-47.

[1985] ZIENKIEWICZ, O. C., VILOTTE, J. P., TOYOSHIMA, S., "Iterative Method for Constrained and Mixed Approximation and Inexpensive Improvement of F.E.M. Performance," *Comput. Appl. Mech. Engrg.* **51**, 3.

[1987] HUGHES, T.J.R., "The Finite Element Method: Linear Static and Dynamic Analysis," Prentice-Hall, Inc., Englewood Cliffs.

[1987] MOLINARI, A., CANOVA, G.R., and AHZI, A., "A Self Consistent Approach of the Large Deformation Polycrystal Plasticity," *Acta Metall.* **35**, 2983.

[1987] WENK, H.R. and KOCKS, U.F., "The Representation of Orientation Distributions," *Metall. Trans.* **18A**, 1082.

[1989] HARREN, S.V. and ASARO, R.J., "Nonuniform Deformations in Polycrystals and Aspects of the Validity of the Taylor Model," *J. Mech. Phys. Solids* **37**, 191.

[1989] MATHUR, K.K. and DAWSON, P.R., "On Modeling the Development of Crystallographic Texture in Bulk Forming Processes," *Int. J. Plast.* **5**, 67.

[1989] MATHUR, K.K. and JOHNSSON, S.L., "The Finite Element Method on a Data Parallel Computing System," *Int. J. High Speed Comp.* **1**, 29.

[1990] KOCKS, U.F., KALLEND, J.S., and BIONDO, A.C., "Accurate Representations of General Textures By a Set of Weighted Grains," Los Alamos National Laboratory LA-UR-90-2828, Los Alamos, NM.

[1990] MATHUR, K.K., DAWSON, P.R., and KOCKS, U.F., "On Modeling Anisotropy in Deformation Processes Involving Textured Polycrystals with Distorted Grain Shape," *Mechanics of Materials* **10**, 183.

[1991] BECKER, R., "Analysis of Texture Evolution in Channel Die Compression - I. Effects of Grain Interaction," *Acta Metall. Mater.* **39**, 1211.

[1991] BRONKHORST, C.A., KALIDINDI, S.R., and ANAND, L., "Evolution of Crystallographic Texture During the Deformation of Fcc Metals," in LOWE, T.C., ROLLETT, A.D. FOLLANSBEE, P.S. and DAEHN, G.S. (eds.), Modeling the Deformation of Crystalline Solids, The Minerals, Metals and Materials Society, Warrendale, pp. 211-223.

[1991] THINKING MACHINES INC., "Connection Machine CM-200 Series Technical Summary," Thinking Machines Corporation, Cambridge, MA.

[1991] JOHAN, Z., HUGHES, T.J.R., MATHUR, K.K., and JOHNSSON, S.L., "A Data Parallel Finite Element Method for Computational Fluid Dynamics on the Connection Machine System," to appear in *Comp. Meth. Appl. Mech. Engrg.*

[1991] KALIDINDI, S.R., BRONKHORST, C.A., and ANAND, L., "On the Accuracy of the Taylor Assumption in Polycrystalline Plasticity," in BOEHLER, J.P. and KHAN, A.S. (eds.), Anisotropy and Localization of Plastic Deformation, Proceedings of Plasticity '91: The Third International Symposium on Plasticity and Its Current Applications, Elsevier, London, pp. 139-142.

[1991] KALLEND, J.S., KOCKS, U.F., ROLLETT, A.D., and WENK, H.-R., "Operational Texture Analysis," *Mat. Sci. Eng.* **A132**, 1.

[1991] SMELSER, R.E. and BECKER, R., "Earing in Cup Drawing of a (100) Single Crystal," in ABAQUS Users' Conference Proceedings, September 1991, Oxford, England, pp. 457-471.

[1992] MATHUR, K.K., BEAUDOIN, A.J., and DAWSON, P.R. in preparation.

A Vector Representation of Deviatoric Tensors

To effect numerical computations, the deviatoric tensors in this work are cast in a 5 element vector form. Accordingly, the fourth-order stiffness and compliance tensors are represented as 5×5 matrices. The following convention is adopted (MATHUR *et al.* [1990])

$$\boldsymbol{D} \equiv \{D\}^T = \{D_{11} - D_{22}, D_{33}, D_{21}, D_{31}, D_{32}\} \tag{30}$$

$$\boldsymbol{P} \equiv \{P\}^T = \{P_{11} - P_{22}, P_{33}, P_{21}, P_{31}, P_{32}\} \tag{31}$$

$$\sigma' \equiv \{\sigma\}^T = \left\{\frac{\sigma_{11} - \sigma_{22}}{2}, \frac{3}{2}\sigma'_{33}, \sigma'_{21}, \sigma'_{31}, \sigma'_{32}\right\} \tag{32}$$

B Development of Orthotropic Material Properties at the Aggregate Level

We wish to show that 4 crystals of equal volume (or weight), undergoing a coaxial deformation, with orientations related by orthorhombic sample symmetry operations, form an orthotropic stiffness matrix. The orthorhombic operations are

$$[O^{(0)}] = \begin{bmatrix} 1 & 0 & 0 \\ 0 & 1 & 0 \\ 0 & 0 & 1 \end{bmatrix} \tag{33}$$

$$[O^{(1)}] = \begin{bmatrix} 1 & 0 & 0 \\ 0 & -1 & 0 \\ 0 & 0 & -1 \end{bmatrix} \tag{34}$$

$$[O^{(2)}] = \begin{bmatrix} -1 & 0 & 0 \\ 0 & 1 & 0 \\ 0 & 0 & -1 \end{bmatrix} \tag{35}$$

$$[O^{(3)}] = \begin{bmatrix} -1 & 0 & 0 \\ 0 & -1 & 0 \\ 0 & 0 & 1 \end{bmatrix} \tag{36}$$

To achieve this an orthotropic response, the four crystals must exhibit identical constitutive behavior. To this end, we require that these crystals share the same slip system hardnesses and that slip system viscosities are developed using the power law relation. These crystals differ in state by orientation only. In the following development, barred quantities are defined the crystal reference frame. In accordance with the Taylor hypothesis, the deformation rate $\overline{D}^{(i)}$ in the crystal reference frame for a crystal associated with the rotation $O^{(i)}$ is

$$\overline{D}^{(i)} = \left(RO^{(i)T}\right) D \left(RO^{(i)T}\right)^T \tag{37}$$

where R is the is a matrix relating the sample coordinate system and the coordinate system of the crystal associated with the identity operation $O^{(0)}$. VANHOUTTE & AERNOUDT [1976] have shown that such two orientations with be equivalent, that is stresses in two lattice frames will equal

$$\overline{\sigma}^{(i)} = \overline{\sigma}^{(j)} \qquad i, j \in \{0, 1, 2, 3\} \tag{38}$$

provided that rotations $O^{(1)}$ and $O^{(2)}$ commute with the sample system deformation rate D. Such is the case in the coaxial deformation and orthorhombic symmetry operations considered in this study. Hence the constitutive behavior developed from the crystal response

$$\overline{\sigma'} = \overline{C} \cdot \overline{D} \tag{39}$$

will be the same for the four equivalent orthorhombically-related orientations.

It will now be shown that the averaged constitutive response derived from the four crystals yields an orthotropic stiffness matrix. We switch to a component notation with no sum implied on any index. The four orthorhombic rotation operators may be written in the abbreviated form

$$o^{(0)} = [1.1.1]^T \tag{40}$$
$$o^{(1)} = [1.-1.-1]^T \tag{41}$$
$$o^{(2)} = [-1.1.-1]^T \tag{42}$$
$$o^{(3)} = [-1.-1.1]^T \tag{43}$$

The averaged stiffness matrix $\hat{c}$ is

$$\hat{c}_{ijkl} = \frac{1}{4} \sum_{m=0}^{3} o_i^{(m)} o_j^{(m)} o_j^{(m)} o_k^{(m)} \bar{c}_{ijkl} \tag{44}$$

or, as $o^{(0)}$ represents the identity operation

$$\hat{c}_{ijkl} = \frac{1}{4} \bar{c}_{ijkl} \left\{ 1 + \sum_{m=1}^{3} o_i^{(m)} o_j^{(m)} o_j^{(m)} o_k^{(m)} \right\} \tag{45}$$

Rewriting the rotation operator

$$o_i^{(m)} = 2\delta_{mi} - 1 \tag{46}$$

where $m \in 1.2.3$ results in

$$\hat{c}_{ijkl} = \frac{1}{4} \bar{c}_{ijkl} \left\{ \sum_{m=1}^{3} (2\delta_{mi} - 1)(2\delta_{mj} - 1)(2\delta_{mk} - 1)(2\delta_{ml} - 1) \right\} \tag{47}$$

Using the definitions

$$\begin{aligned} \delta_{ijkl} &= 1 && \text{if } i = j = k = l \\ &= 0 && \text{otherwise} \end{aligned} \tag{48}$$

and

$$\begin{aligned} \delta_{ijk} &= 1 && \text{if } i = j = k \\ &= 0 && \text{otherwise} \end{aligned} \tag{49}$$

and expanding eqn (47) gives

$$\begin{aligned} \hat{c}_{ijkl} = \frac{1}{4} c_{ijkl} [&(\delta_{ij} + \delta_{ik} + \delta_{il} + \delta_{jk} + \delta_{jl} + \delta_{kl} - 1) \\ &-2(\delta_{ijk} + \delta_{ijl} + \delta_{ikl} + \delta_{jkl}) + 4\delta_{ijkl}] \end{aligned} \tag{50}$$

We are interested in the zero components of $\hat{c}_{ijkl}$.

- For components relating a normal stress component to a shear deformation component ($i = j$ and $k \neq l$) eqn (50) reduces to

$$\hat{c}_{ijkl} = c_{ijkl} [(\delta_{ik} + \delta_{il} + \delta_{jk} + \delta_{jl}) - 2(\delta_{ijk} + \delta_{ijl})] \tag{51}$$

  which is zero. A similar result for components $\hat{c}_{ijkl}$ relating shear stress components with normal deformation components follows from the major symmetry of $\hat{c}_{ijkl}$.

- For those components $\hat{c}_{ijkl}$ relating two shear stress components eqn (50) becomes

$$\hat{c}_{ijkl} = c_{ijkl} [(\delta_{kl} + \delta_{il} + \delta_{jk} + \delta_{jl} - 1)] \tag{52}$$

  which will be non-zero only if

  1. $i = k$ and $j = l$. or,
  2. $i = l$ and $j = k$

  Due to symmetry of the deformation rate and stress tensors, this is a statement that a shear stress component will be related only to the corresponding shear deformation rate component through the stiffness tensor $\hat{c}_{ijkl}$.

Hence the stiffness tensor resulting from the averaged response of the four orientations is orthotropic.

Figures

1. Layout of crystals on parallel architecture
2. Undeformed and deformed specimens
3. Initial specimen texture prior to deformation
4. Normalized cross-sectional velocity magnitude after final simulation time step
5. Crystal Orientation Distribution (COD) polar cross-sections of simulated and experimental texture after deformation
6. {100} pole figures of simulated and experimental texture after deformation

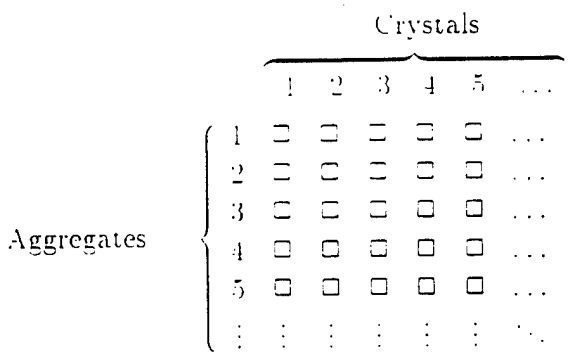

Figure 1

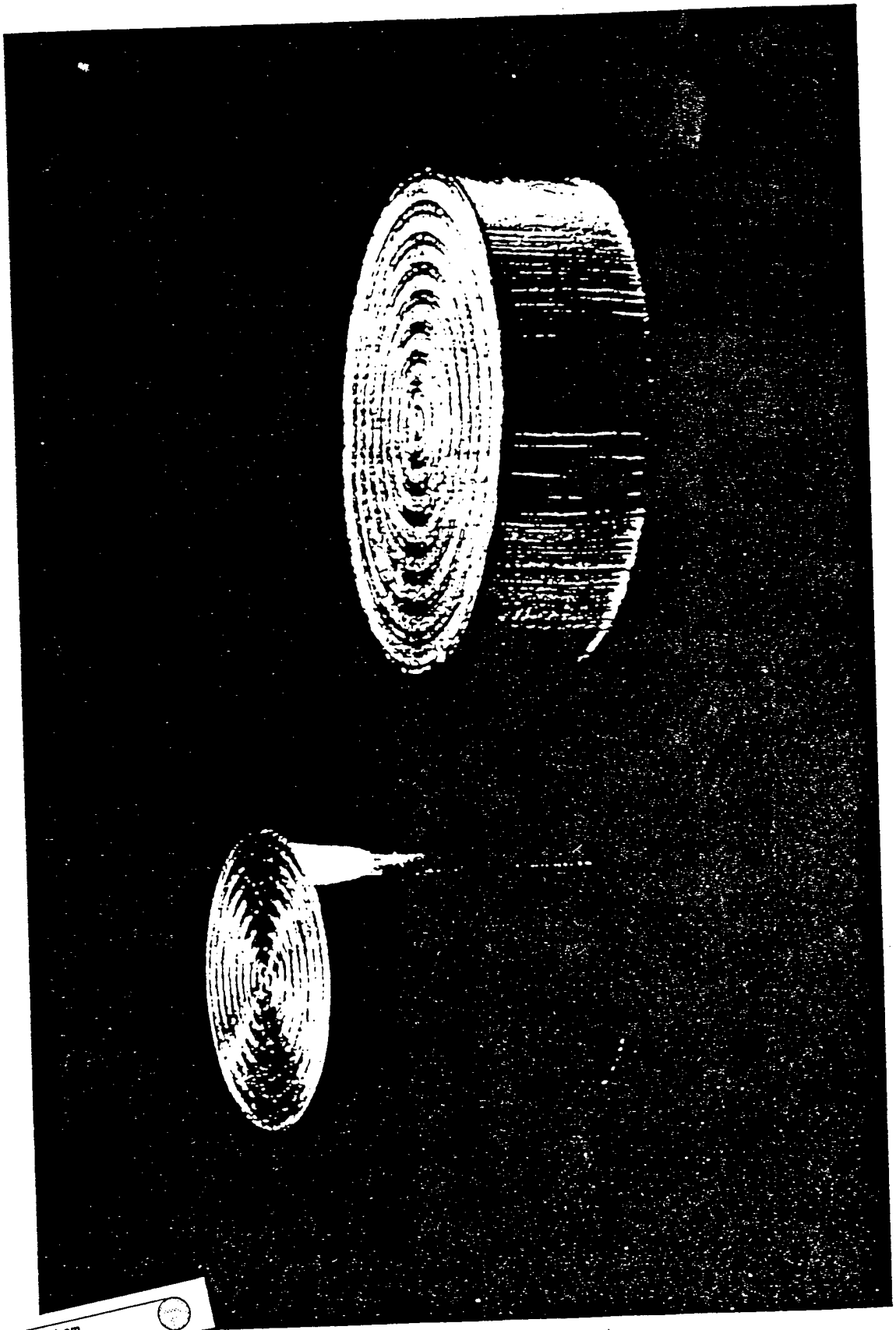

Figure 2

Normalized Cross-sectional Velocity Magnitude

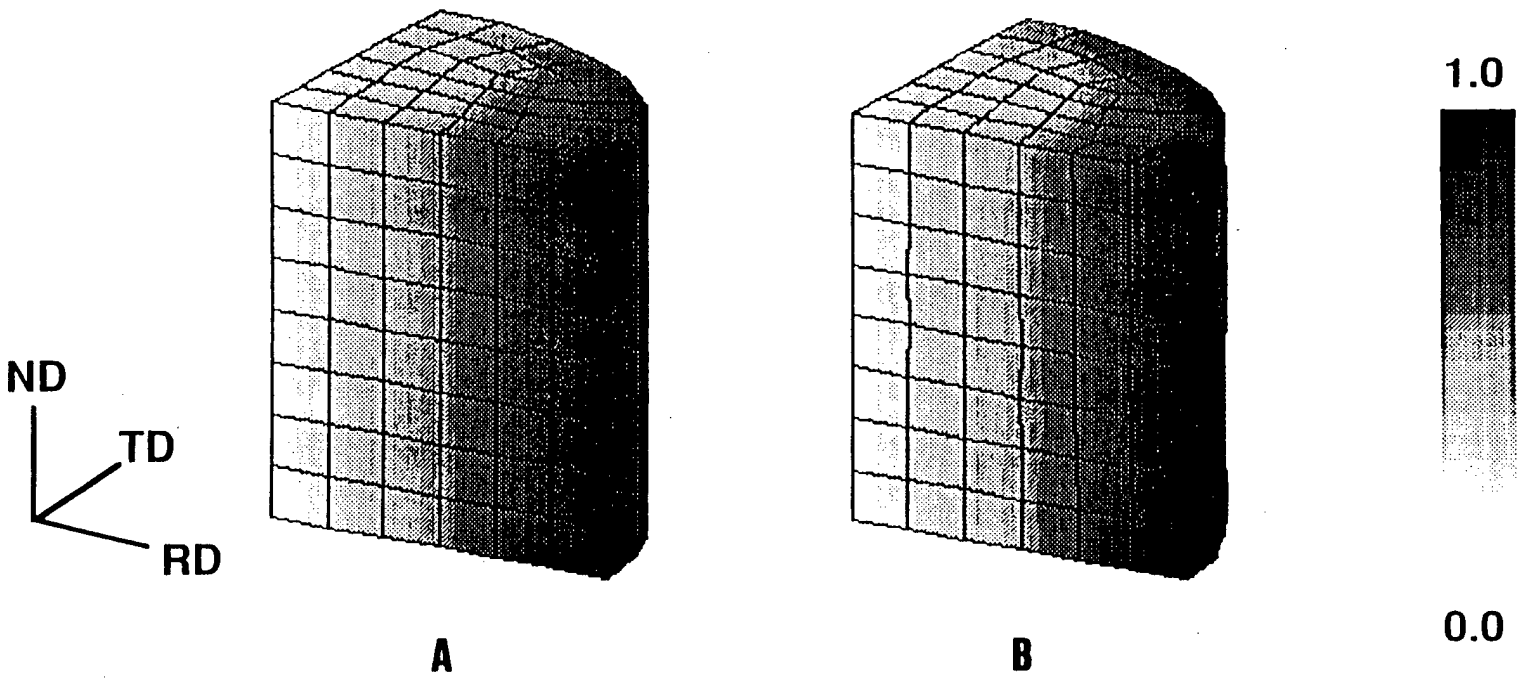

47

Figure 4

ndcor2 .WTS file from texcub 18-JAN-92 , Smoothed 5

CODK min = 4; max = 486; last median = 0

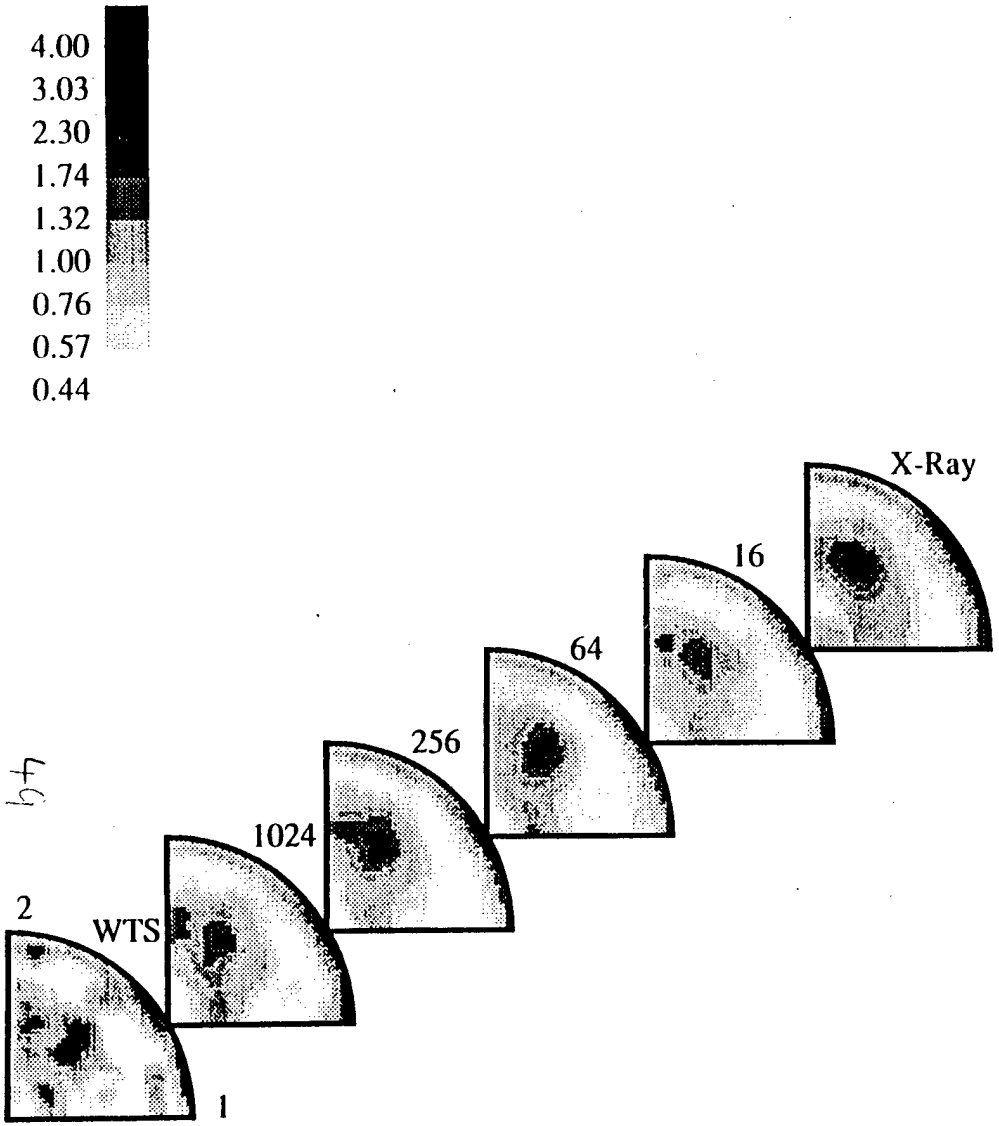

Figure 6

Reproduced by NTIS